

# Geochemistry, Geophysics, Geosystems

## RESEARCH ARTICLE

10.1029/2018GC008054

### Key Points:

- Record of snow petrel occupation history in Antarctica goes back to >58 ka (thousand years before present)
- The small-scale and singular mumiyo deposits preserve intact stratigraphy
- Mumiyo deposits are archives of past environmental conditions in Antarctica

### Supporting Information:

- Supporting Information S1

### Correspondence to:

S. Berg,  
sberg0@uni-koeln.de

### Citation:

Berg, S., Melles, M., Hermichen, W.-D., McClymont, E. L., Bentley, M. J., Hodgson, D. A., & Kuhn, G. (2019). Evaluation of mumiyo deposits from East Antarctica as archives for the Late Quaternary environmental and climatic history. *Geochemistry, Geophysics, Geosystems*, 20, 260–276. <https://doi.org/10.1029/2018GC008054>





Received 1 NOV 2018

Accepted 15 DEC 2018

Accepted article online 18 DEC 2018

Published online 11 JAN 2019

## Evaluation of Mumiyo Deposits From East Antarctica as Archives for the Late Quaternary Environmental and Climatic History

S. Berg<sup>1</sup> , M. Melles<sup>1</sup>, W.-D. Hermichen<sup>2</sup>, E. L. McClymont<sup>3</sup> , M. J. Bentley<sup>3</sup> , D. A. Hodgson<sup>3,4</sup>, and G. Kuhn<sup>2</sup> 

<sup>1</sup>Institute of Geology and Mineralogy, University of Cologne, Cologne, Germany, <sup>2</sup>Alfred-Wegener-Institut Helmholtz-Zentrum für Polar- und Meeresforschung, Bremerhaven, Germany, <sup>3</sup>Department of Geography, Durham University, Durham, UK, <sup>4</sup>British Antarctic Survey, Cambridge, UK

**Abstract** Mumiyo deposits form in the vicinity of snow petrel (*Pagodroma nivea*) nesting sites and consist of fossil stomach oil (mumiyo), guano, and minerogenic material. Here we evaluate mumiyo deposits from the inland mountain ranges of central Dronning Maud Land as high-resolution archives for paleoenvironmental reconstructions in Antarctica. Investigation of internal structures and chemical composition shows that the lamination reflects progressive sedimentation, despite the irregular outer morphology of the deposits. Detailed radiocarbon analysis demonstrates that stratigraphies are intact: <sup>14</sup>C ages become successively younger upwards in the deposits. Fatty acid and *n*-alcohol composition was determined on samples from eight mumiyo deposits. Dominance of low molecular weight compounds (C<sub>14</sub> to C<sub>18</sub>) points to a dietary signal; however, the relatively low proportions of unsaturated compounds compared to fresh stomach oils indicates some postdepositional degradation. We found marine diatoms in the mumiyo, which potentially provide a proxy for sea ice conditions in the foraging habitat of the petrels. Age ranges of the investigated deposits suggest occupation of the analyzed sites by snow petrels from 17 ka to >58 ka. Changes in deposition rates point to higher occupation frequency in Petermann Range from 46 to 42 ka compared to the late marine isotope stage 3 and the Last Glacial Maximum.

## 1. Introduction

Many ice-free terrestrial sites on the Antarctic continent and offshore islands are colonized by snow petrels (*Pagodroma nivea*) during the breeding season from November to March (Croxall et al., 1995; Delord et al., 2016; Figure 1). Snow petrels use sheltered rock cavities in bedrock or under moraine boulders as nesting sites (Einoder et al., 2014). Uniquely for sea birds of the order procellariiformes, they produce stomach oil, which serves as energy storage during long-distance flights between the hunting area in the open ocean and the nesting sites and for chick feeding (Warham, 1977). Snow petrels also eject the oil against intruders to defend the nests (e.g., against predatory skuas and competitors). Over periods of decades to millennia, this leads to the accumulation of stomach oil, so-called Antarctic mumiyo, in the vicinity of the nests (e.g., Ainley et al., 2006; Hiller et al., 1988). In the cold and dry climates on the continent the stomach oil deposits are preserved and thus provide a record of snow petrel occupation in the past.

Initial radiocarbon (<sup>14</sup>C) dating of mumiyo deposits proved the datability of the organic material (e.g., Hiller et al., 1988). The <sup>14</sup>C ages of mumiyo deposits provide age constraints on the timing of deglaciation or inundation of terrestrial sites, since mumiyo deposition at a given time implies subaerial exposure, that is, neither ice or snow coverage nor flooding by lake or ocean (e.g., Kiernan et al., 2002; Wand & Hermichen, 2005), and thereby can complement exposure dating of glacial erratics and landforms in Antarctica (Mackintosh et al., 2011). In currently unglaciated coastal areas of East Antarctica, like Bunger Hills, Vestfold Hills, and Larsemann Hills, as well as from more inland sites in the Prince Charles Mountains and Shackleton Range, mumiyo ages indicate a snow petrel colonization predominantly during the Holocene, following local deglaciation (e.g., Ainley et al., 2006; Hiller et al., 1988; Kiernan et al., 2002, 2009; Mackintosh et al., 2011; Verkulich & Hiller, 1994; Figure 1).

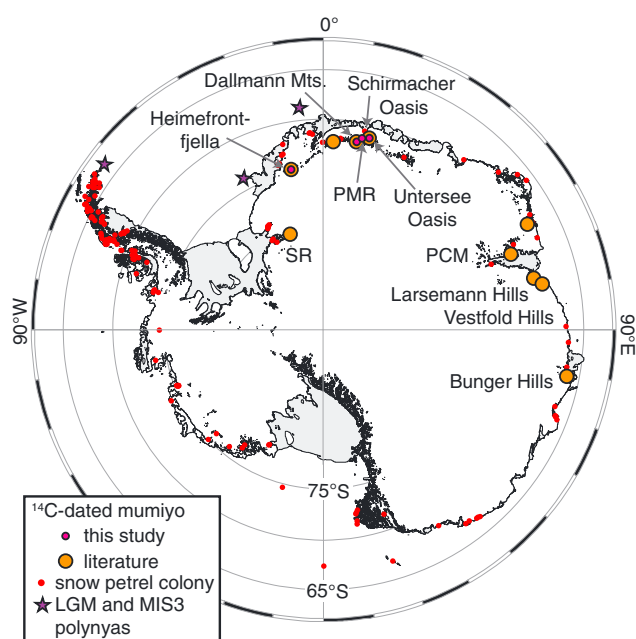


**Figure 1.** Modern distribution of snow petrel breeding colonies (Croxall et al., 1995; Goldsworthy & Thomson, 2000; Steele & Newton, 1995) and locations of  $^{14}\text{C}$ -dated mumiyo deposits (Hiller et al., 1988; Kiernan et al., 2002; Kiernan et al., 2009; Mackintosh et al., 2011; Melles et al., 1997; Ryan et al., 1992; Steele & Hiller, 1997; Thor & Low, 2011; Verkulich & Hiller, 1994; Wand & Hermichen, 2005). SR = Shackleton Range; PMR = Petermann Range; PCM = Prince Charles Mountains. Stars indicate locations of marine sediment records, which suggest polynyas during the Last Glacial Maximum (LGM) and marine isotope stage 3 (MIS3; Smith et al., 2010; Sprenk et al., 2014; Thatje et al., 2008).

Mumiyo ages of up to 37 thousand years before present (ka) were found in the mountain ranges of western and central Dronning Maud Land (DML), indicating snow petrel occupation and of ice-free sites during the late Pleistocene (Hiller et al., 1988, 1995; Steele & Hiller, 1997; Thor & Low, 2011; Figure 1).

The spatial and temporal pattern of snow petrel colonization in East Antarctica also reflects paleoenvironmental changes related to their foraging habitat in the Southern Ocean. The snow petrels depend on productive foraging grounds within flight distance to the colonies in austral summers (e.g., Goldsworthy & Thomson, 2000) and feed in the pack ice, at the northernmost sea ice margin or in polynyas (Ainley et al., 1984; Ballard et al., 2012; Delord et al., 2016). During glacial periods, like the Last Glacial Maximum (LGM, 26.5 to 19 ka; Clark et al., 2009), most of these areas were likely covered by perennial sea ice (Gersonde et al., 2005). However, coastal polynyas occurred in some areas off East Antarctica (Smith et al., 2010; Sprenk et al., 2014), which may explain the occurrence of snow petrel colonies in DML during the LGM (Hiller et al., 1988; Thatje et al., 2008) and suggests that these regions were important refuges for Antarctic biota during glacial periods (Thatje et al., 2008; Younger et al., 2016). Hence, mumiyo deposits can provide unique information on the coastal ocean, which may not be preserved or reflected in marine sediment records from the respective areas. Furthermore, the composition of mumiyo may reflect changes in diet over time, a dependency that has repeatedly been shown for ornithogenic deposits from penguin rookeries (e.g., Emslie & Woehler, 2005; Gao et al., 2018). However, there is only one study so far, in which stable isotope data of organic carbon and hydrogen from mumiyo deposits in Bunger Hills were used to reconstruct Holocene changes in the food web off the East Antarctic coast (Ainley et al., 2006; Figure 1).

Here we present a multidisciplinary investigation of pre-Holocene mumiyo in Antarctica. The major intention of our study is to evaluate to what extent the mumiyo deposits can be used as a high-resolution archive for paleoenvironmental reconstructions in Antarctica. The deposits investigated have thicknesses of up to 45 cm and originate from central DML (Figure 1). Laboratory work comprised (i) studies of the internal structure to examine the three-dimensional stratigraphy of individual deposits, (ii) detailed radiocarbon dating to extend the data set of historic snow petrel settlement and determine changes in deposition rates, (iii) high-resolution X-ray fluorescence (XRF) elemental scans and C, N, and S analyses to characterize the chemical composition, (iv) analyses of fatty acids (FAs) and *n*-alcohols to investigate the potential of lipid biomarkers as an indicator for changes in prey composition, and (v) determination of diatoms in the mumiyo as a potential proxy for sea ice conditions in the foraging habitat of the petrels.

## 2. Materials and Methods

The mumiyo samples originate from the Dallmann Mountains, Petermann Range, and Untersee Oasis, and from Scharffenbergbotnen (Heimefrontfjella; Figure 1). Long-term storage of the samples was at 4 °C. The mumiyo was frozen (−20 °C) immediately prior to subsampling in order to prevent deformation of the resinous material, which melts at room temperature.

Analytical work was carried out on two sample types, namely, (a) samples from profiles throughout mumiyo sections (PRM10 and DallSW1830) and (b) samples from the base and from the surface of 12 mumiyo blocks (Table 1).

From the base and surface samples lipids were separated from clastic particles by extraction with a Soxhlet apparatus in preextracted cellulose-extraction thimbles with 500-ml DCM:MeOH (9:1) for 24 hr. The resulting total lipid extract (TLE) was saponified and neutral lipids were separated by partitioning the TLE in deionized water (MilliQ) and Dichloromethane (DCM). The *n*-alcohols (FALc) were

**Table 1**  
*List of Mumiyo Deposits Used in This Study*

Sample name	Max. thickness (mm)	Expedition	Region	Coordinates	Altitude (m a.s.l.)	Altitude above ice margin (m)
PRM4	250	GeoMaud 1995/1996	Petermann Range	71°22'S/ 12°35'E	1,450	280
PRM6	70	GeoMaud 1995/1996	Petermann Range	71°22'S/ 12°35'E	1,190	320
PRM8	180	GeoMaud 1995/1996	Petermann Range	71°21'S/ 12°36'E	1,420	250
PRM10	180	GeoMaud 1995/1996	Petermann Range	71°22'S/ 12°35'E	1,490	320
WMM3.2	450	GeoMaud 1995/1996	Untersee Oasis	71°22'S/ 13°19'E	1,460	895
WMM7	170	GeoMaud 1995/1996	Untersee Oasis	71°22'S/ 13°19'E	880	320
WMM11	100	GeoMaud 1995/1996	Untersee Oasis	71°20'S/ 13°22'E	1,150	590
WMM14	200	GeoMaud 1995/1996	Untersee Oasis	71°22'S/ 13°23'E	950	300
Dall E-II/1	150	GeoMaud 1995/1996	Dallmann-Berge, E	71°43'S/ 10°16'E	1,730	30
DallSW1830-2	150	GeoMaud 1995/1996	Dallmann-Berge, SW	71°46'S/ 10°11'E	1,830	130
SB-I/1a	190	ANT-XV/2 1997/1998	Scharffenbergbotnen/ Heimefrontfjella	74°35'S/ 11°13'E	1,350	150
SB-XI/1g	130	ANT-XV/2 1997/1998	Scharffenbergbotnen/ Heimefrontfjella	74°33'S/ 11°16'W	1,295	35

*Note.* Maximum thicknesses of the deposits and information on the sampling campaign and sample locations are given. A table with complete metadata is available on PANGAEA (doi:10.1594/PANGAEA.847318).

purified from the neutral lipids by open-column chromatography and acetylated prior to analysis with a gas chromatograph (Agilent 7890B, Agilent Technologies, USA), employing a flame ionization detector equipped with a 50-m DB5 MS column (0.2 mm i.d. and 0.33- $\mu$ m film thickness by Agilent Technologies, USA). Identification and quantification were done using authentic external standards (C16 to C24). FAs were separated from the residual TLE by acidification with HCl to pH 1 and separated by liquid-liquid separation, methylated, and purified by open-column chromatography as described by Höfle et al. (2013). For identification of positions of double bonds in unsaturated compounds they were separated from saturated compounds by open-column chromatography with SiO<sub>2</sub> coated with AgNO<sub>3</sub> and eluted with ethyl acetate. A split of the unsaturated fraction was dissolved in Hexane and derivatized with dimethyl-disulfide (DMS). Identification was achieved by GC-MS (single quadrupole mass spectrometer HP 5989 coupled with a HP 5890 gas chromatograph, both Hewlett Packard). Quantification of FA methyl esters (FAMES) was done by GC-FID (Flame ionization detector, Agilent 7890B, Agilent Technologies, USA) using authentic external standards (FAME-mix C8-C24 [CRM18918] and BAME-mix [47080-U] both Sigma Aldrich).

For diatom analysis, residual material insoluble in organic solvents of six samples was treated with HCl (10%) and hydrogen peroxide (30%) to remove carbonates and organic matter, respectively. Identification and counting of diatoms were made on permanent slides (Naphrax) with a Zeiss Axio Scope A1 at 1,000X magnification.

The mumiyo profiles became accessible after cutting the deposits vertically with a band saw (diamond blade). On the profiles, high-resolution line-scan images were recorded and XRF analysis was carried out with an ITRAX XRF core scanner (Cox Analytical Systems, Sweden). XRF analyses were conducted with a chromium X-ray tube (settings 30 kV and 55 mA), an exposure time of 20 s, and a resolution of 500  $\mu$ m. A principal component analysis was applied to the inorganic elemental dataset using the

**Table 2**  
*Radiocarbon Ages of Mumiyo Samples*

Region	Sample ID	Depth (mm)	Lab code	<sup>14</sup> C age (years BP)	Age (cal years BP)
Petermann Range	PRM4-top	surface	COL3020	40,660 ± 370	42,670–43,980
Petermann Range	PRM4-top	surface	AWI-272	38,000	—
Petermann Range	PRM4-A	190–192	COL4532	>58,000	—
Petermann Range	PRM8-1	surface (10–15)	COL4323	22,000 ± 112	24,840–25,570
Petermann Range	PRM8-A	10–12	COL4761	15,735 ± 60	17,620–17,990
Petermann Range	PRM8-A	20–22	COL4760	21,940 ± 90	24,760–25,460
Petermann Range	PRM8-A	40–42	COL4759	39,420 ± 300	42,000–42,850
Petermann Range	PRM8-A	60–62	COL4757	42,230 ± 380	43,855–45,351
Petermann Range	PRM8-A	80–82	COL4756	46,470 ± 560	47,548 to >50,000
Petermann Range	PRM8-A	100–102	COL4755	52,090 ± 1000	—
Petermann Range	PRM8-A	120–122	COL4754	>56,000	—
Petermann Range	PRM8-A	140–142	COL4753	>56,000	—
Petermann Range	PRM6-A	0–2	COL4521	28,550 ± 150	31,060–31,500
Petermann Range	PRM6-1	base	COL4321	>58,000	—
Petermann Range	PRM10-2	surface (0–10)	COL4315	17,650 ± 80	19,685–20,190
Petermann Range	PRM10-4	base	COL4316	42,860 ± 490	44,270–46,010
Petermann Range	PRM10-A	10–12	COL4515	17,160 ± 70	19,160–19,590
Petermann Range	PRM10-A	40–42	COL4516	21,950 ± 90	24,790–25,490
Petermann Range	PRM10-A	70–72	COL4517	38,530 ± 209	41,505–42,210
Petermann Range	PRM10-A	100–102	COL4518	41,460 ± 380	43,200–44,660
Petermann Range	PRM10-A	130–132	COL4519	43,330 ± 440	44,730–46,340
Petermann Range	PRM10-A	150–152	COL4520	43,870 ± 470	45,106–46,960
Untersee Oasis	WMM7-top	surface	COL3022	21,551 ± 110	24,250–25,021
Untersee Oasis	WMM7-top	surface	AWI-279	21,200	—
Untersee Oasis	WMM14-3	base	COL4317	45,070 ± 560	45,950–48,550
Untersee Oasis	WMM11-2B	10–15	COL4319	30,745 ± 180	33,490–34,120
Untersee Oasis	WMM11-2A	base	COL4318	43,074 ± 490	44,445–46,190
Dallmann Mts.	DallSW1830	surface	AWI-277	4,900	—
Dallmann Mts.	DallSW1830	base	AWI-276	18,200	—
Dallmann Mts.	Dall E-II/1	base	AWI-172	3,440	—
Heimefronfjella	SB-XI/1g-A3	base	COL4320	5,248 ± 40	4,620–4,840
Heimefronfjella	SB-I/1a	0–10	COL3021	1,885 ± 40	650–824
Heimefronfjella	SB/1-1a	0–10	AWI-275	1,400	—

*Note.* Samples labeled with COL were measured by AMS at the CologneAMS and samples labeled AWI were measured by LSC spectrometry at the Alfred Wegener Institute in Potsdam. Ages were calibrated with Calib 7.10 (Stuiver & Reimer, 1993) and the calibration data set Marine13.14 (Reimer et al., 2013) with a constant marine reservoir correction of 1,100 years. Calibrated ages are given as 95% confidence ranges. Samples PRM8-A and PRM10-A are from vertical cross sections, while basal and surface samples were taken from the exterior of the respective deposits. AMS = accelerator mass spectrometry.

PAST3 program (Hammer et al., 2001), in order to relate the element profiles to changes in composition.

Additional information concerning the chemical composition of the mumiyo profiles was obtained by analysis of total carbon (C), total nitrogen (N), and total sulfur (S) contents. Measurements were conducted with a vario microcube (Elementar, Germany) on 2-mm-thick subsamples of the profiles. Due to the sticky consistence of the material the samples could not be homogenized prior to analysis. Consequently, each sample was measured in four replicates of ~2.5 mg each, and the mean values ± standard deviations were calculated.

Both the base and surface samples from the mumiyo deposits and samples from the inner parts of one mumiyo profile were dated by radiocarbon analyses on bulk material, which was treated with dilute HCl to remove carbonates prior to analysis. Most samples (lab codes starting with COL, Table 2) were graphitized with an automated graphitization system (AGE, Wacker et al., 2010) and analyzed for <sup>14</sup>C by accelerator mass spectrometry (AMS) at the CologneAMS, Germany (Dewald et al., 2013). Samples with lab codes starting with AWI (Table 2) were analyzed for <sup>14</sup>C at the radiocarbon laboratory of



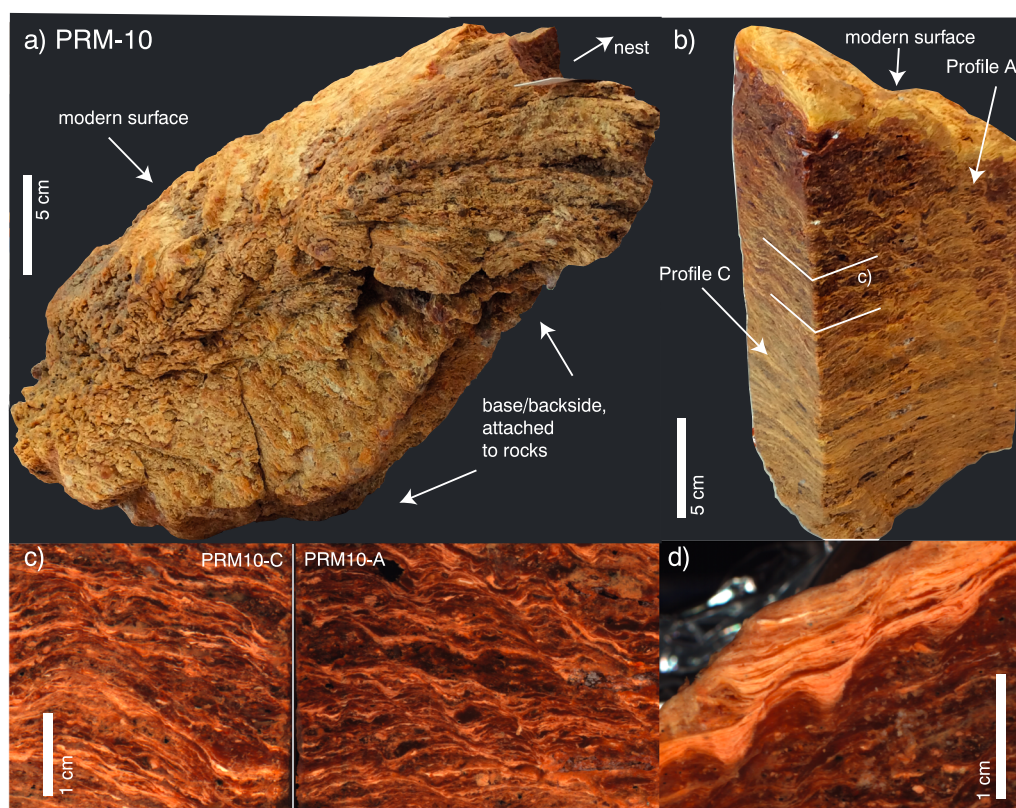


**Figure 2.** Mumiyo deposit PRM10 prior to subsampling (a) and after cutting longitudinal profiles, which were used for lithological and structural descriptions as well as further analyses (b). (c) Close-ups of profiles PRM10-C and PRM10-A (for location see b) illustrating the three-dimensional structure of the deposit and (d) close-up of the yellowish surface layers, which likely are a weathering feature.

the Alfred Wegener Institute in Potsdam, Germany. There, total organic carbon was combusted and the evolving  $\text{CO}_2$  was converted to benzene following standard procedures (Polach et al., 1972), and the  $^{14}\text{C}$  activity was measured using a Packard TRI-CARB 2560 TR/XL liquid scintillation spectrometer.

### 3. Results and Discussion

#### 3.1. Lithology

Due to the formation in front of different nesting cavities and between rocks the 12 mumiyo deposits have rather individual, irregular shapes (Figures 2a and S1 in the supporting information). They have maximal thicknesses of 70 to 450 mm (Table 1). At their bases, mumiyo-encrusted feathers and incorporated rock fragments and sand particles represent the initial stage of their formation. The surfaces of the deposits are uneven and wrinkled. This could be due to irregular formation, but it could also be an effect of degradation as a consequence of microbial activity and/or physical weathering initiated by desiccation (Hiller et al., 1988). In general, siliciclastic mineral grains and rock fragments in mumiyo deposits derive from bedrock in the surroundings of the nests. Larger clasts incorporated in the deposits likely originate from the weathered cave walls and roofs or indicate dislocation of the whole deposit, followed by further deposition. Grains of sand and silt size, which were found in varying proportions in the extraction residues of the mumiyo samples, could as well be redeposited by wind transport and by the birds landing and sitting on top of the deposits.

Despite the irregular shapes of the whole deposits, the internal structure shows distinct layering and, in some deposits, even lamination on millimeter to sub-millimeter scale (Figures 2 and 3). The layers are represented by changes in color, which likely are due to different proportions of stomach oil, mineral grains, and guano. The variability in the internal structure becomes evident from more detailed descriptions of cross

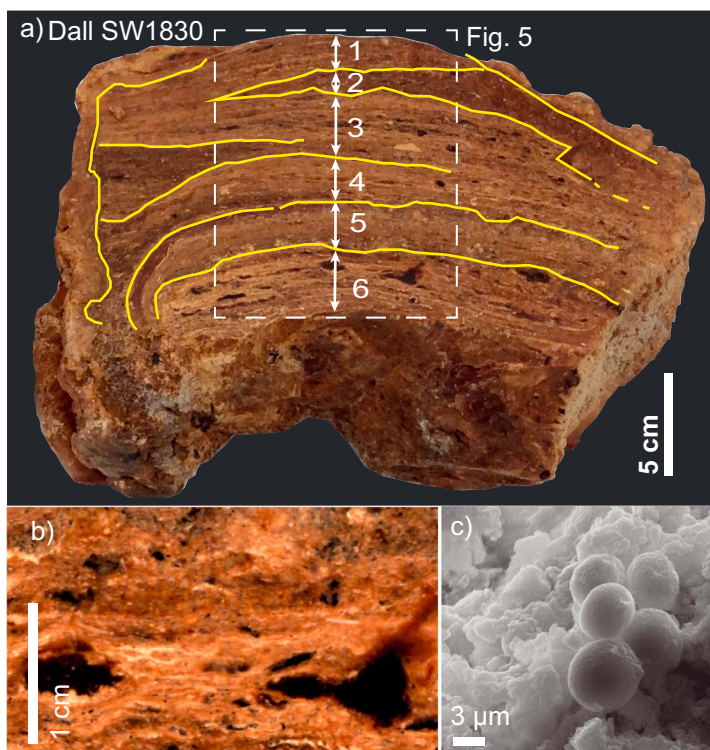


**Figure 3.** (a) Mumiyo deposit DallSW1830 after cutting longitudinal profiles, which were used for lithological and structural descriptions as well as further analyses. Yellow lines highlight structural features, arrows and numbers 1 to 6 indicate position of XRF profile and lithological units and hatched line indicates mumiyo part presented in Figure 5 in more detail. (b) Close-up of internal structures; note black nodules in the lower part. (c) Scanning electron microscope image of urate nodules found in the basal layers of PRM10.

sections of the mumiyo deposits PRM10 from Petermann Range and DallSW1830 from Dallmann Mountains. The descriptions include three-dimensional correlations of visible structural features to study the extent of layers and to identify possible discontinuities and hiatuses, which have to be considered in interpreting paleoenvironmental conditions.

*PRM10.* The mumiyo deposit PRM10 has an inclined surface (Figures 2a and 2b). This results in profiles of varying thickness in the block cut from the deposit (profile A: 180 mm, B: 180 mm, C: 190 mm, D: 150 mm; Figures 4 and S2). The bottom and backside of the deposit, which were originally attached to the rock surface, are covered with white salt efflorescence, sand, rock fragments, feathers, and bones. The mumiyo material is brownish and orange in color, with the exception of the undulated, yellowish present-day surface (Figure 2d). The surface may reflect a weathering rind, which progressively forms from the outer margins of the deposit during prolonged exposure and possibly leads to successive degradation and erosion of the mumiyo over time (Figure 2d). In general, the internal structure of PRM10 is finely laminated (Figures 2b–2d). While the submillimeter scale laminae are discontinuous and often confine wedges and lenses, some prominent thicker layers are continuous in lateral extent on centimeter scale and can be tracked in all four profiles (Figure 2c).

The downcore changes in texture and color correlate between the profiles A to D, allowing subdivision of the deposit into four stratigraphic units (Figures 4 and S2). In the lower part (unit 4), the layers are almost horizontal and do not resemble the outer shape of the deposit. The orientation of the layers becomes more inclined in the upper part (Units 3 to 1). Due to the three-dimensional internal structure this effect is less pronounced in profiles PRM10-C and PRM10-D, which are oriented perpendicular to the inclined surface. The varying thickness of the units within the deposit likely results from the irregular grounds the deposit was initially formed on, the irregular paleo-surfaces (similar to the current surface) and the patchy nature of accumulation.

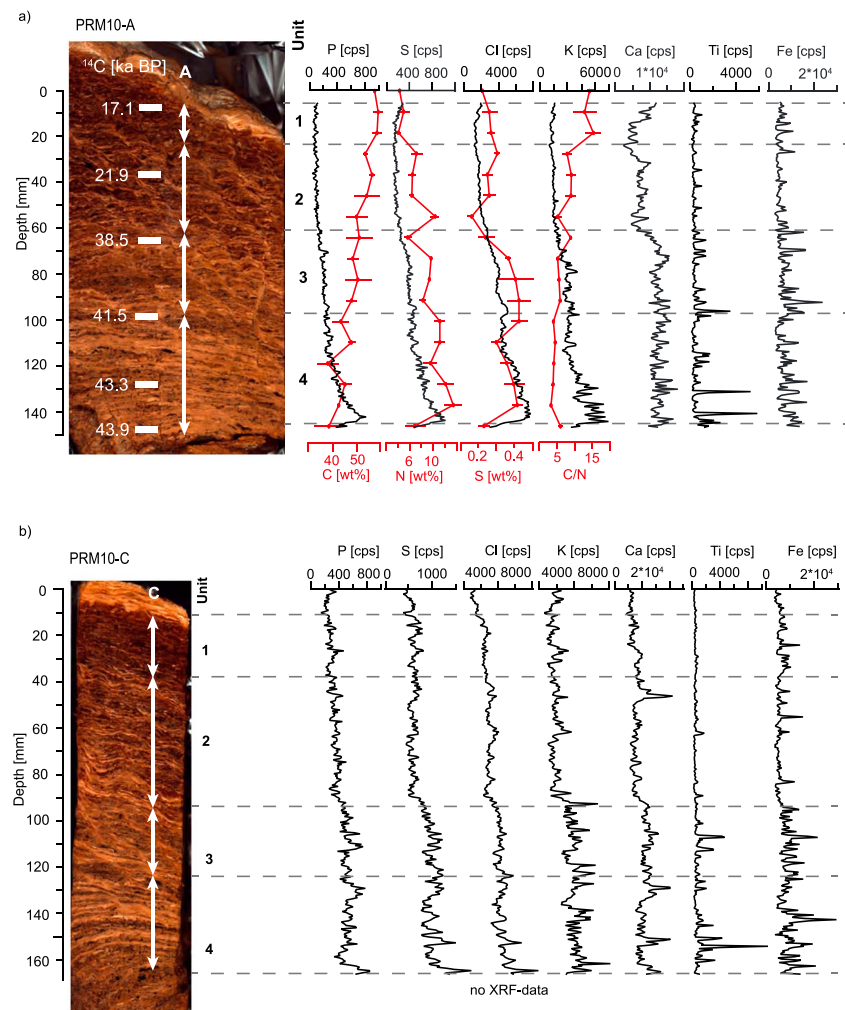


**Figure 4.** Line-scan images of mumiyo profiles PRM10-A (a) and PRM10-C (b). Arrows indicate units defined in the profile and also mark the position of X-ray fluorescence elemental scans. In profile A, the positions of subsamples for  $^{14}\text{C}$  analysis and the  $^{14}\text{C}$  ages are indicated. Results of X-ray fluorescence elemental scans are given as counts per second (cps).

*DallSW1830.* The mumiyo deposit DallSW1830 (Figure 3) was collected in front of a bouldery moraine (Wand & Hermichen, 2005). It has a maximum thickness of ~160 mm and a wrinkled, grayish, brownish surface. In parts, the deposit is covered by molten material, which probably is not an original feature but formed after sample collection.

Cross sections reveal that DallSW1830 is internally layered (Figure 3a; plate 1 in Wand & Hermichen, 2005). The surface is part of a layer that crosscuts the internal layering. This may reflect that the deposit was in a state of degradation and not accumulation when it was sampled and that the surface consequently is a weathering feature. Alternatively, the surface and the layer below could be a depositional feature, marking the rather recent onset of deposition after a period of erosion or nondeposition.

Based on the internal structures DallSW1830 was divided into six lithological units (Figure 3a). The variable thicknesses of the layers indicate wedge-like structures and some of the boundaries between the units likely reflect discontinuities in deposition. The basal part (unit 6) is of light color and contains interspersed black nodules of up to 1 cm in diameter (Figures 3b and 5). The contact with the following unit 5 is likely erosive, since unit 5 contains more siliciclastic grains and reworked mumiyo layers. Units 4 to 2 show layering; however, structures on millimeter to submillimeter scale are discontinuous and point to disturbance shortly after deposition (hence prior to burial by subsequent material), for instance, due to the birds landing on the surface or due to physical processes like desiccation or abrasion (Figures 3b and 5). In unit 1 small-scale



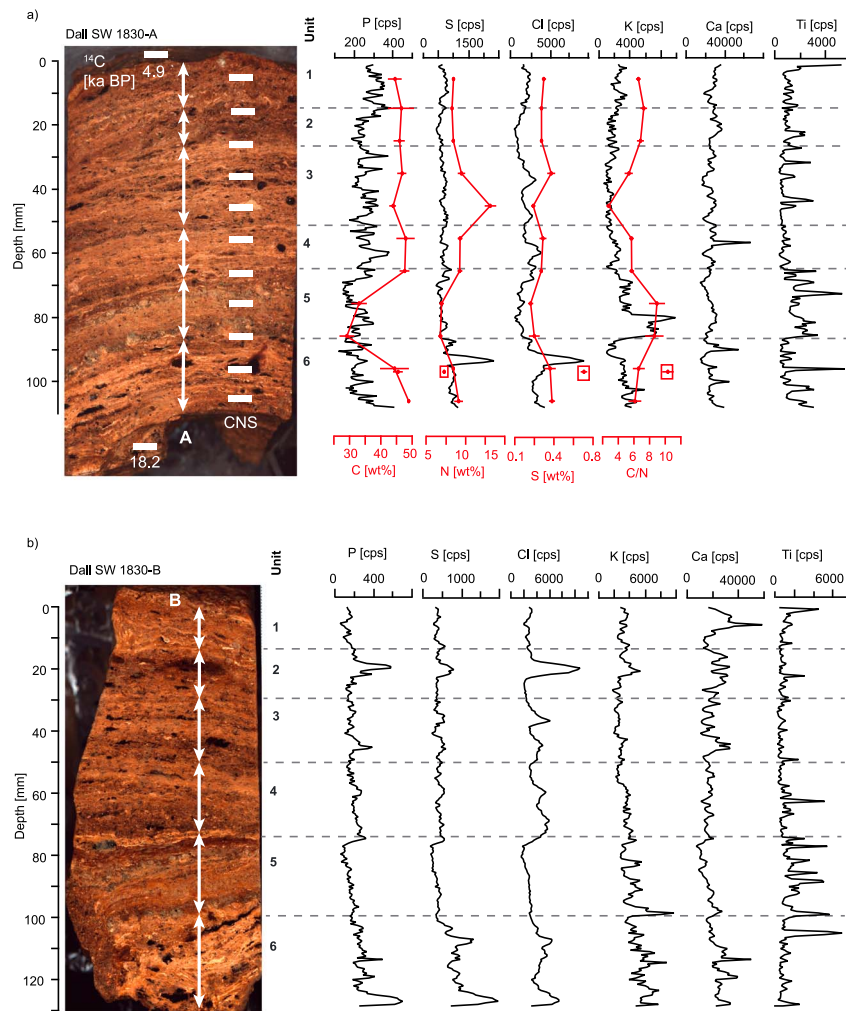


**Figure 5.** Line-scan images of mumiyo profiles DallSW1830-A (a) and DallSW1830-B (b). Arrows indicate units and also mark the position of X-ray fluorescence elemental scans. In profile A, the positions of subsamples for  $^{14}\text{C}$  and CNS analysis and the  $^{14}\text{C}$  ages are indicated. Results of X-ray fluorescence elemental scans are given as counts per second (cps). Red boxes in (a) indicate CNS values obtained from black nodules (cf. Figure 3b).

structure indicates a reworking horizon similar to unit 5, which is in accordance with the large-scale structure (truncation of unit 2; Figure 3a).

### 3.2. Elemental Analyses

Analyses of total carbon (C), total nitrogen (N), and total sulfur (S) were conducted on 17 subsamples of profile PRM10-A (Figure 4a). C contents range from  $37.6 \pm 4.7$  to  $59.2 \pm 2.0$  wt% and N contents from  $3.9 \pm 0.5$  to  $13.3 \pm 1.6$  wt%. C contents are lowest in the basal part of the profile and increase upwards, while N contents show a decreasing trend. This is also reflected by the C/N ratio, which increases from  $\sim 5$  in unit 4 to  $\sim 15$  in the uppermost unit 1 (Figure 4a). Sections with high C and low N contents (high C/N ratio) are likely rich in stomach oil lipids (triglycerides and wax esters), which do not contain N. High N concentrations, in contrast, reflect the incorporation of guano, since bird guano contains up to 50% nitrogenous compounds like uric acid ( $C_5H_4N_4O_3$ ; C/N ratio = 1.1), chitin, proteins, and ammonia (e.g., Haus et al., 2016; Lindeboom, 1984). S contents range from  $0.16 \pm 0.02$  to  $0.43 \pm 0.05$  wt%, with higher values ( $>0.3$  wt%) in units 4 and 3 and low values ( $<0.3$  wt%) in units 2 and 1, and may reflect changes in guano concentration (Roberts et al., 2017).

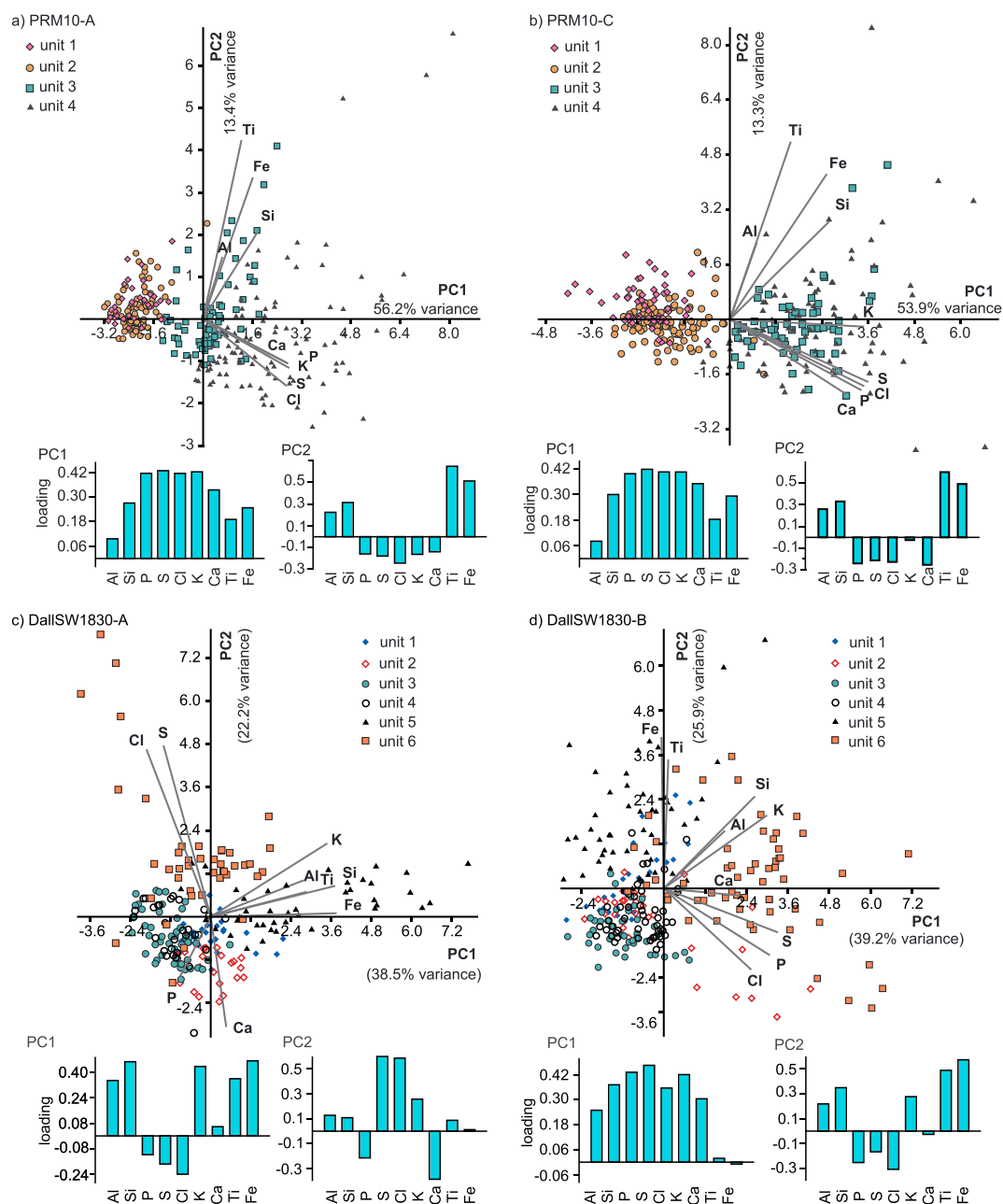


**Figure 6.** Biplot loadings PC1 and PC2 of X-ray fluorescence data for profiles PRM10-A (a) and PRM10-C (b), and DallSW1830-A (c) and DallSW1830-B (d), along with loadings of the respective elements for PC1 and PC2. Scores of subsamples of each profile are color coded for lithological units defined in Figure 4 (PRM10) and Figure 5 (DallSW1830).

In 11 subsamples of profile DallSW1830-A C contents range from  $29.0 \pm 2.4$  to  $48.9 \pm 2.0$  wt%, N contents from  $3.4 \pm 0.5$  to  $16.3 \pm 1.6$  wt%, and S contents from  $0.16 \pm 0.03$  to  $0.71 \pm 0.03$  wt% (Figure 5a). C contents are around 45 wt% throughout the profile, with distinctly lower values occurring in unit 5 only. These low C contents likely reflect higher proportions of non-carbon-bearing siliciclastic material, which dilutes the carbon derived from stomach oil and guano.

XRF elemental scans of Al, Si, P, S, Cl, K, Ca, Ti, and Fe were obtained on profiles PRM10-A to PRM10-D (Figures 4 and S2) and DallSW1830-A to DallSW1830-C (Figures 5 and S2). In both deposits changes in element counts broadly correspond to the units defined in the lithological descriptions. Principal component



analysis of the XRF data indicates correlation of Al, Si, Ti, and Fe that reflect the siliciclastic component, hence mineral grains like aluminosilicates (Figures 6 and S3). Ti and Fe profiles show distinct peaks (Figures 4, 5, and S2), which point to intervals of enrichment of both elements, for instance, due to interspersed mineral grains. Higher proportions of siliciclastic matter occur, for example, in unit 5 of DallSW1830 (Figure 5) and units 4 and 3 in PRM10 (Figure 4).

The organic component is only indirectly reflected in the XRF data, since XRF elemental scanning does not detect light elements like C and N, which are the main constituents of the mumiyo deposits. In deposit PRM10, element XRF peak counts show a general trend of decreasing values upwards, while the proportion of C and N increase (Figures 4 and S2). This dilution effect is also reflected by principal component PC1, explaining 56.2% and 53.9% of variance in profiles PRM10-A and PRM10-C, respectively (Figures 6a and 6b).

The correlation of elements P, S, and Cl point to a marine, likely biogenic source (e.g., Huang et al., 2008; Liu et al., 2013) and most likely reflect the incorporation of snow petrel guano (Figure 6). In PRM10 there is some variability between the profiles A to D, however, relatively high concentrations of guano in units 4 and 3 are indicated by high values in Cl, S, and P (Figures 4 and S2). In DallSW1830 pronounced peaks in Cl and S in unit 6 and partly in unit 2 (Figures 5 and S2) correspond to black nodules found throughout the deposit (Figure 3b). Other elements are not enriched in the nodules, except P, which is higher in some cases, like at 20-mm depth in DallSW1830-B (Figure 5b). The absence of higher Ca counts argues against bones or carbonates as an origin of the nodules. However, the material could be remnants of bones or carbonate fossils after dissolution of the inorganic matrix under low pH, leading to enrichment of organic C, S, and Cl.

In the investigated profiles the elements K and Ca show affinity to the siliciclastic as well as the guano-related elements (Figures 6 and S3). In DallSW1830-A and DallSW1830-B, for example, Ca and P correlate (negative loadings in PC2; Figures 6c and 6d), which could be explained by the occurrence of hydroxylapatite or fluorapatite ( $\text{Ca}_5(\text{PO}_4)\text{F}$ ). In deposit PRM10, K and Ca likewise correlate with guano elements. Aside from siliciclastic aluminosilicates, K and Ca deposits are likely bound to authigenic phosphates in both deposits, comparable to those which form in ornithogenic soils associated with penguin rookeries. There, weathering products of guano and mineral detritus react and form a variety of K- and Ca-bearing phosphates (e.g., Pereira et al., 2013; Roberts et al., 2017). The mineral detritus available for the formation of authigenic phosphates probably differs in composition in DallSW1830 and PRM10, explaining the different correlation patterns for K and Ca and influencing the amount and type of phosphates formed after deposition. In ornithogenic soils in Antarctica, the formation of phosphates depends on the availability of water and is sensitive to the pH of the weathering solution (Mychra & Tatur, 1991; Pereira et al., 2013). The formation of such minerals in the vicinity of snow petrel nests indicates that moisture is available to form weathering solutions. Inland areas are dry and cold and the nesting sites of snow petrels are often on north facing slopes (Hiller et al., 1995). There, particularly high insolation likely leads to local warming of rock and mumiyo surfaces and episodic melting of snow and ice, which provides water for weathering reactions. In penguin rookeries the pH of the weathering solution is controlled by the microbial degradation of guano, which leads to the conversion of uric acid into oxalic acid and a successive lowering of pH (Haus et al., 2016). During the initial stages of guano degradation urates, struvite  $[(\text{NH}_4)\text{MgPO}_4 \cdot 6(\text{H}_2\text{O})]$ , fluorapatite  $[\text{Ca}_5(\text{PO}_4)\text{F}]$ , and brushite  $[\text{Ca}(\text{PO}_3(\text{OH})) \cdot 2(\text{H}_2\text{O})]$  form under alkaline to neutral conditions (Mychra & Tatur, 1991). Successive lowering of pH leads to formation of K-phosphates like minyulite  $[\text{KAl}_2(\text{PO}_4)_2(\text{OH},\text{F}) \cdot 4(\text{H}_2\text{O})]$ , taranakite  $[\text{K}_3\text{Al}_5(\text{HPO}_4)_6(\text{PO}_4)_2 \cdot 18(\text{H}_2\text{O})]$ , and leucophosphate  $[\text{KFe}_2(\text{PO}_4)_2(\text{OH}) \cdot 2\text{H}_2\text{O}]$  (Mychra & Tatur, 1991; Pereira et al., 2013). Apart from differences in the initial composition of mineral detritus, the supposed presence of K-phosphates in PRM10 as opposed to DallSW1830, where Ca phosphates seem to dominate, could reflect a difference in the degree of guano weathering between the deposits.

### 3.3. Radiocarbon Analysis

A total of 27 AMS measurements was conducted on 9 mumiyo deposits (Table 2). AMS  $^{14}\text{C}$  ages from surficial samples of three deposits are very similar to ages measured on the same deposits by Liquid Scintillation Counting spectrometry (PRM4-top, WMM7-top and SB I/1a; Table 2). These similarities indicate that both methods provide reproducible  $^{14}\text{C}$  dates on mumiyo deposits. The existing age differences may result from sample inhomogeneity, since the analyses were not carried out on identical aliquots. They may also be

due to differences in sample mass, which is much larger (5 g C) for Liquid Scintillation Counting spectrometry compared to AMS analyses (~1 mg C).

The range of ages we determined on the mumiyo deposits is from 1.4  $^{14}\text{C}$  ka BP to infinite, corresponding to >58 ka (Table 2). Top and basal ages of deposits DallSW1830, PRM4, PRM6, PRM8, and PRM10 were analyzed to assess the age ranges of the deposits. All four deposits from Petermann Range have pre-Holocene ages, ranging from a minimum age of 22.0  $^{14}\text{C}$  ka BP (PRM8-1) to infinite (>58  $^{14}\text{C}$  ka BP; PRM4-A and PRM6-1), while the deposit DallSW1830 from the Dallmann Mountains ranges from 18.2 to 4.9  $^{14}\text{C}$  ka BP (Table 2).

Additionally,  $^{14}\text{C}$  ages of 2-mm-thick samples were obtained for profiles PRM8-A and PRM10-A (Table 2). In PRM10 top and basal ages are in accordance with samples taken from the irregularly shaped exterior of the deposit and span an age range of about 25,000 years. Six ages from the well-laminated profile PRM10-A become consistently older with depth (ranging from 17.6 to 43.6  $^{14}\text{C}$  ka BP). Similar results were found for profile PRM8-A, which spans an age range from 15.8 to >58  $^{14}\text{C}$  ka BP (Tables 2 and S1). The age of sample PRM8-1 (22.0  $^{14}\text{C}$  ka BP) that was taken from the subsurface elsewhere in the deposit (S1) coincides with the age at 20 mm depth in profile PRM8-A (21.9  $^{14}\text{C}$  ka BP), likely reflecting the spatial variability in thicknesses of individual layers. The  $^{14}\text{C}$  ages suggest that the visually identifiable layers and horizons in the mumiyo represent isochrones similar to layers in other sedimentary deposits. Mean deposition rates vary distinctly over time. For instance, the  $^{14}\text{C}$  ages of PRM10-A show that the lower 6 cm cover ~2,500 years (corresponding to ~24 mm/ka), while the upper 7 cm comprise >20,000 years (~3.5 mm/ka). In PRM8, the deposition rate varies, between 7.1 mm/ka (60- to 40-mm depth) and 1.3 mm/ka (40- to 10-mm depth). Changes in deposition rates likely correlate to the frequency of nest occupation. Aside from low accumulation due to less frequent occupation, abandonment of the nests may lead to degradation/weathering and erosion of the subaerially exposed mumiyo, resulting in apparently low accumulation. Although the internal structure in PRM10 does not clearly evidence unconformities or mechanical disturbance, additional, high-resolution  $^{14}\text{C}$ -dating could help to distinguish periods of very low accumulation from hiatuses caused by erosion.

### 3.4. Diatom Analysis

All six samples analyzed for diatoms contain diatom frustules or fragments of frustules (Table S1). However, in the samples from PRM6 and PRM8 diatom concentrations are low and the frustules are not well preserved, whereas from WMM11 only unidentifiable fragments were found. In samples from PRM10 and Dall E-II/1 the frustules are well preserved and 15 species were identified (Table S1). The assemblages in these deposits are dominated by *F. curta* and *F. cylindrus*, which comprise 21.4% to 56.8% and 7.7% to 39.6% of the counted diatoms, respectively. Both species are marine, associated with sea ice and frequently occur in coastal areas of Antarctica and within the winter sea ice zone of the Southern Ocean (Zielinski & Gersonde, 1997). Other sea-ice-related diatom taxa identified in the mumiyo samples are *F. ritscheri*, *F. obliquecostata*, and *F. sublinearis*. The open-ocean species *F. kerguelensis*, which comprises 6.5% to 23.8% in the analyzed samples, is frequent in pelagic areas north of the winter sea ice edge, reaching maximum abundances at water temperatures between 0 and 10 °C (Zielinski & Gersonde, 1997).

The diatoms in the mumiyo are likely supplied by the snow petrels, which ingest krill and other diatom-feeding organisms, and excrete undigested diatoms at the nesting site as reported for penguins (Mychra & Tatur, 1991). Some alteration of the diatom species composition in mumiyo deposits compared to the surface ocean may occur due to selective preservation. Heavily silicified frustules could be enriched, since they are more resistant to dissolution and/or breakage than delicately silicified diatoms. The three most abundant species in the mumiyo samples (*F. kerguelensis*, *F. curta*, and *F. cylindrus*) have heavily silicified frustules and are well preserved in the sediment record of the Southern Ocean (e.g., Zielinski & Gersonde, 1997).

### 3.5. Lipid Analysis

Eleven samples were analyzed for FAs (Figure 7) and *n*-alcohols (FALc; Table S2). FALc and FA are likely derived from wax esters, which are major constituents in fresh stomach oil of snow petrels (Warham et al., 1976) and monoglycerides and free FAs, which have additionally been found in fossil mumiyo (Aiello et al., 2011). The dominant FA homologues are 16:0, 14:0, and 18:0 (Figure 7), comprising  $33.7 \pm 6.0$ ,  $16.9 \pm 3.3$ , and  $6.4 \pm 1.1\%$  of the FAs, respectively. The most abundant homologues for the

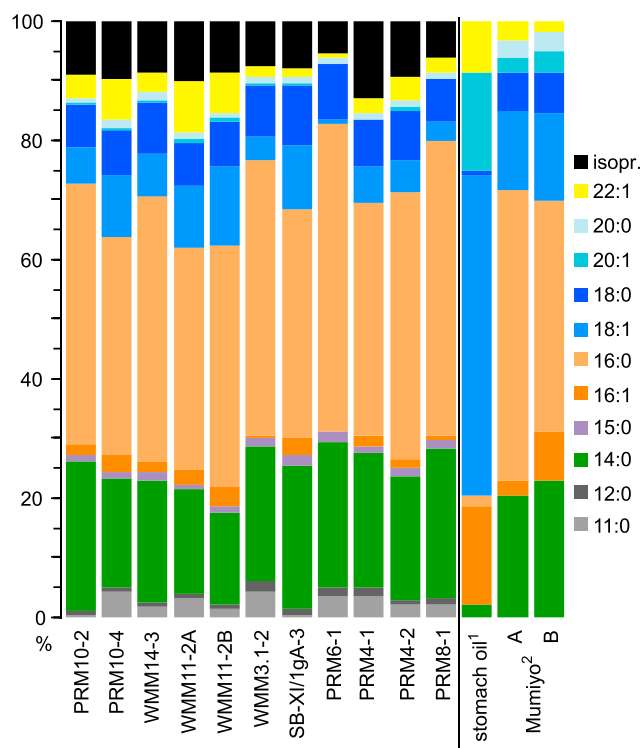


**Figure 7.** *n*-Fatty acids identified in mumiyo. For comparison, the compositions of (1) fresh stomach oil of snow petrels from Northern Victoria Land (Warham et al., 1976) and of a (2) Holocene mumiyo deposit from Schirmacher Oasis are shown (A: fatty acids in monoglycerides B: free fatty acids; Aiello et al., 2011).

FALCs are 16:0, 14:0, and 18:0 as well ( $71.8 \pm 1.5$ ,  $19.9 \pm 1.9$ , and  $5.3 \pm 1.5\%$ ), which show only minor variability between the samples. Monounsaturated FAs (MUFAs) comprise 1.4% to 24.2% (mean  $13.5 \pm 6.9\%$ ) of FAs and contain 16:1, 18:1 (mainly 18:1 $\Delta$ 9), 20:1 $\Delta$ 11, 22:1 $\Delta$ 11, and 22:1 $\Delta$ 13.

The FA and FALC composition we find in the fossil material differs from fresh stomach oils of snow petrels and other procellariiformes by low proportions of unsaturated compounds. MUFAs and PUFAs contribute ~50% to >95% of FAs in fresh stomach oils (e.g., Connan et al., 2007, 2008; Warham et al., 1976). The mumiyo has lower proportions of  $C_{18}$  and higher proportions of  $C_{16}$  and  $C_{14}$  compounds than fresh stomach oils. The ratio of  $C_{18}/C_{16}$  compounds in mumiyo ranges from 0.2 to 0.5 and is higher in stomach oils of snow petrels (~2.7; Watts & Warham, 1976) and other procellariiform birds (e.g., 2.3 for *Halobaena caerulea*; Connan et al., 2008). Although these differences might reflect a diet specific to DML, the FA patterns of organisms snow petrels generally feed on show higher  $C_{18}/C_{16}$  ratios as well (1.0 for *Euphausia superba*, 0.9 to 1.9 for *Electrona antarctica*, 2.9 for *Gonatus antarcticus*; Lea et al., 2002; Phleger et al., 1997, 2002; Phillips et al., 2002). Higher proportions of  $C_{16}$  and  $C_{14}$  relative to  $C_{18}$  are reported for phytoplankton (e.g., diatoms, Nichols et al., 1993). The isoprenoid FAs 2,6,10,14-tetramethylpentadecanoic acid (phytanic acid) and 3,7,11,15-tetramethylhexadecanoic acid (pristanic acid) were identified in the mumiyo ( $2.7 \pm 0.5\%$  and  $3.2 \pm 1.3\%$ , respectively). Both compounds are chlorophyll derivatives, which have been assigned to conversion products of dietary phytol (Hansen & Meiklen, 1970). Both compounds have been found in herbivorous Antarctic krill (*E. superba*) and krill feeding Antarctic whales (Hansen & Meiklen, 1970). Preservation of phytanic acid in triglycerides in stomach oils has been demonstrated for *Puffinus tenuirostris* (Short-tailed shearwater)

(Connan et al., 2005). The relatively high proportions of isoprenoid FAs and relatively high proportions of  $C_{14}$  and  $C_{16}$  relative to  $C_{18}$  could be an indicator for a specific diet of snow petrels in DML consisting of organisms of lower trophic levels (e.g., herbivorous krill).

The high proportion of saturated compounds in the fossil mumiyo points to alteration, likely by subaerial oxidation, UV radiation, and microbial degradation causing loss of the more easily degradable MUFAs and PUFAs. For our sample set the proportion of MUFAs does not correlate with the age of the samples, indicating that other factors than time affect the hydrogenation of FAs. Such factors could include differences in original stomach oil composition, deposition rate, temperature, moisture availability, and UV radiation, which control the duration of exposure as well as the intensity of microbial activity on and in the deposits. Iso and anteiso branched 15:0 and 17:0 FAs are generally assumed as bacterial markers and have been found in mumiyo in concentrations of  $\leq 0.6\%$  (Table S2). This concentration is similar to that of myctophid fish (Lea et al., 2002) and Antarctic euphausiids (Hansen & Meiklen, 1970; Phleger et al., 2002), which are components of snow petrel diet (e.g., Ferretti et al., 2001). Hence, iso and anteiso 15:0 and 17:0 FAs levels in the mumiyo are not significantly elevated compared to a potential dietary source and are not indicative for bacterial activity specifically in the terrestrial deposits.

#### 4. Environmental History

Our  $^{14}\text{C}$  analyses show that mumiyo deposits in central DML have formed and been preserved over a time period of more than 58,000 years. The overlapping age ranges of the individual deposits indicate continuous or recurrent snow petrel colonization of the Petermann Range and Untersee Oasis during this period (Figure 8a). On shorter timescale (decades) temporary abandonment of a specific cavity could result from the death of at least one individual of a breeding pair. A lack of occupancy can be accompanied by temporary filling of the cavity with snow and ice, and it no longer being attractive to potential prospecting petrels. On

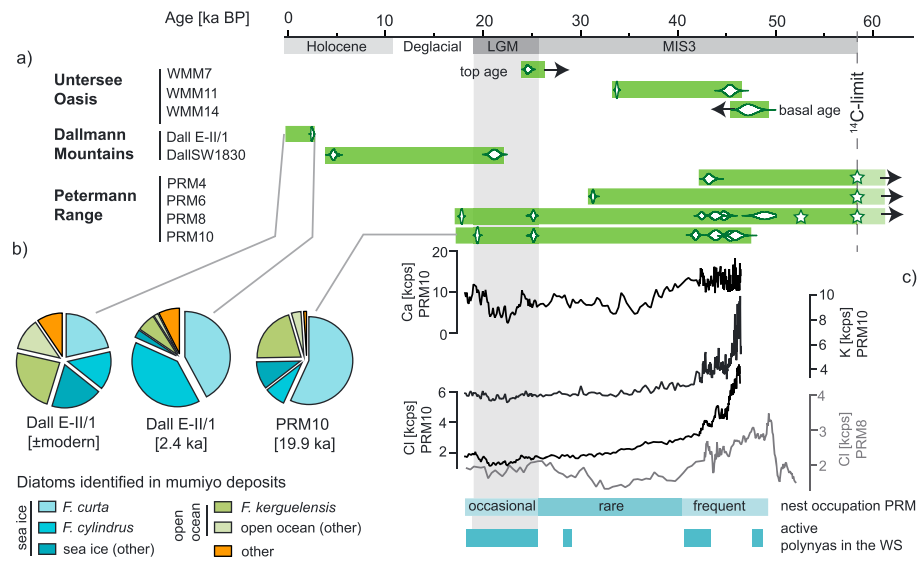


**Figure 8.** (a) Preliminary paleoenvironmental interpretation of mumiyo deposits from central Dronning Maud Land. Green bars show age ranges of mumiyo deposits dated for this study (cf. Table 2). Calibrated ages are given as 95% confidence ranges, stars indicate uncalibrated ages (either infinite  $^{14}\text{C}$  value or exceeding calibration curve). (b) Diatom composition of three samples (cf. Table S1). (c) X-ray fluorescence elemental scans for Ca and K (given as kilo counts per second [kcps] and elemental peak area) for PRM10-A and Cl (kcps) for PRM10-A and PRM8, with preliminary age models created by linear extrapolation between dated horizons. (c) Timing of active polynyas in the eastern and western Weddell Sea (WS) derived from marine sediment records (Smith et al., 2010; Sprenk et al., 2014). LGM = Last Glacial Maximum.

longer timescales (centennial to millennial) changes in deposition rates may reflect changes in the number of snow petrels breeding in the region and in the proportion of potential nesting cavities that are actually occupied by breeding petrels. High deposition rates at the sites PRM10 and PRM8 suggest frequent snow petrel occupation between ~42 and 46 cal ka BP, which could be due to a relatively large number of breeding snow petrels and high occupation rates of available nesting cavities in the area. Very low accumulation between ~25 and 42 cal ka BP on the other hand points to rare occupation by snow petrels. The  $^{14}\text{C}$  ages obtained from the deposits DallSW1830, WMM7, PRM10, and PRM8 indicate breeding snow petrels in the mountain ranges also during the LGM (Figure 8a). Holocene mumiyo records are abundant in the Dallmann Mountains and Untersee Oasis (e.g., Wand & Hermichen, 2005). The lack of Holocene deposits in Petermann Range is likely a bias due to the sampling strategy, which focused on the maximum thickness of the deposits and their appearance of “looking old.”

Our data suggest that changes in the terrestrial environment can be derived from the inorganic composition of the deposits. In the basal part of PRM10, high K counts (Figure 8b) likely indicate increased amounts of K relative to Ca phosphates. This probably reflects more intensive guano weathering due to increased bacterial activity and higher availability of water, for instance, due to snow melt. The composition of weathering products of guano could either reflect microenvironments specific for the individual deposits or regional changes in environmental conditions. This relationship needs to be further investigated.

Enrichment in siliciclastic grains is reflected by high Ti and Fe counts and low carbon contents (Figures 4 and 5). High availability of sand- to silt-sized detrital material in the surroundings of the nests as well as high accumulation of guano and stomach oil may support increased accumulation of siliciclastic material. This is suggested by deposit DallSW1830, in which siliciclastic matter is enriched in unit 5 (Figure 5), which was likely was deposited during the deglacial period (~18 to 12 cal ka BP; Figure 8a). Hence, warming and surficial melting may have led to increased supply and redeposition of siliciclastic material in the surroundings of the nesting site. In PRM10, the  $^{14}\text{C}$  ages reflect particularly high accumulation rates in units 4 and 3 (~46–42 cal ka BP, Figure 8a). In this units higher siliciclastic content goes along with high guano content (high Cl counts, low C/N ratios; Figure 4a), indicating frequent nest occupation. Consequently, windblown mineral grains may have better been captured by burial during mumiyo deposition.

During periods of low deposition, exposure of the mumiyo surface did not lead to accumulation of wind-transported material nor did enrichment of clasts by weathering and degradation of the organic matrix probably take place. This is indicated by the deposit PRM10, in which a low accumulation between ~40 and 19 cal ka BP is accompanied by low amounts of siliciclastic matter and guano, and by high proportions of stomach oil (low overall XRF-counts; Figure 8b). The same pattern is visible in the record from PRM8, which shows a decline in guano content (reduced Cl counts) after ~40 cal ka BP (Figure 8b). An explanation could be very cold and dry conditions, which have led to physical weathering and removal of the guano, as well as selective preservation of the stomach oil component. The scarcity in siliciclastic material in PRM10 may also indicate temporary burial of the deposit by windblown snow and ice, which may have reduced the deposition of mineral particles and could also have resulted in the abandonment of the nesting cavity (Einoder et al., 2014).

It is well known that FA signatures of organisms (e.g., crustaceans, myctophid fish, and copepods) differ in their patterns of MUFAs and PUFAs and can be used to distinguish dominant prey organisms in procellariiform stomach oils (e.g., Clarke & Prince, 1976; Connan et al., 2008; Phleger et al., 1997, 2002; Quillfeldt et al., 2011; Williams & Buck, 2010). Lipid analysis in this study revealed that alteration of FAs in the mumiyo likely led to some loss in information on prey constituents by loss of characteristic double bonds. Changes in the proportion of isoprenoid FAs could be an alternative indicator for food composition of snow petrels and may reflect relative changes in the proportion of krill feeding. For example, different FA patterns (e.g., ratio of  $C_{18}$  to  $C_{16}$  compounds) in snow petrel stomach oil from birds living at Cape Hallet, Northern Victoria Land (Watts & Warham, 1976) compared to mumiyo from DML (this study and Aiello et al., 2011; Figure 7) may reflect the different prey composition of snow petrels feeding over the continental shelf in the Ross Sea (Ainley et al., 1984) compared to feeding over the deep ocean in DML, where the shelf is very narrow (Ainley et al., 1992). The differences within the Holocene to >58-ka samples from DML are smaller than those to the Northern Victoria Land stomach oils further highlighting the possibility of regional differences in diet (Figure 7).

Although some information might be lost due to selective preservation, diatoms in mumiyo provide a record of sea ice conditions during the summer months (breeding season) in the foraging area. Snow petrels are closely associated with sea ice (Barbraud et al., 2000; Barbraud & Weimerskirch, 2001) and preferably feed in loose pack ice (Ainley et al., 1984). Less sea ice and more open water species in the surface sample ( $\pm$  modern) relative to deeper in the profile (corresponding to 2.4 cal ka BP) in Dall E-II/1 (Figure 8d) likely reflects temporal changes in sea ice conditions (e.g., increased sea ice concentrations) and a more northward position of the summer sea ice edge 2.4 cal ka BP ago (Ainley et al., 2006). During the LGM, summer sea ice was even more extensive and reached beyond the present-day winter sea ice edge in the Atlantic sector of the Southern Ocean (e.g., Gersonde et al., 2005). In sample PRM10-2, which was dated to the LGM, open-ocean diatoms comprise ~25% of the counted diatoms. The mumiyo record and the accessory diatoms indicate the occurrence of areas with loose sea ice in the foraging range of the snow petrels during and before the LGM. Today, a recurring polynya system exists in the eastern Lazarev Sea, off central DML, ~200 km from the sampling sites (Arrigo & van Dijken, 2003). Frequent snow petrel occupation of the terrestrial sites in DML between 46 and 42 cal ka BP may point to active polynyas in the region. Although polynyas are not exclusively necessary for snow petrels (Ballard et al., 2012), reduced sea ice coverage in the polynya during winter may have led to favorable foraging conditions in the pack ice in the marginal zones of the postpolynya during summer. Polynyas during this interval are also suggested for the Weddell Sea (Smith et al., 2010; Spreng et al., 2014; Figure 8c).

## 5. Conclusions and Outlook

We show that the small-scale and singular mumiyo deposits can preserve intact stratigraphy, which is a precondition for their use as high-resolution archives of past environmental conditions. Detailed analyses of internal structures, chemical composition and  $^{14}\text{C}$  ages reveal that temporal resolution varies within and between deposits. The deposition rate of millimeters to centimeters per thousand years likely reflects the occupation frequency of individual nests allowing for estimates of changes in snow petrel population over time.



By comparing several mumiyo records, we identified potential proxies for further investigations and obtained a first regional interpretation for the late Pleistocene. The ages of the deposits from the northern Petermann Range (central DML) as well as the age range of the deposits from central DML indicate occupation by snow petrels for more than 58,000 years. Guano and products of guano-diagenesis (e.g., urates and phosphates) incorporated in the mumiyo deposits probably contain information on local conditions like temperature and moisture availability, which control microbial activity and guano degradation. In spite of nest-specific variables (e.g., exposure to solar insolation, wind, and deposition rate) two mumiyo profiles from Petermann Range show similar trends in accumulation rates and guano concentration over time. This points to frequent snow petrel occupation between 46 and 42 cal ka BP, while the mountains of Petermann Range were likely rarely visited by breeding snow petrels during the LGM.

Accessory diatoms reflect the foraging of snow petrels in close association with sea ice and could be useful to identify past changes in the marine habitat with respect to sea ice (e.g., to distinguish feeding in loose pack ice from feeding at the large-scale sea ice edge or in polynyas). The food composition is likely reflected by the lipid composition (FAs and *n*-alcohols) of the fossil stomach oils. However, we found some alteration of lipids in the fossil material compared to fresh stomach oil leading to some loss of information on prey composition. Systematic differences in FA patterns between mumiyo (Holocene to >58 ka) from DML as opposed to fresh stomach oils from Northern Victoria Land likely reflect regional characteristics of foraging over the deep ocean in DML as opposed to foraging over a broad continental shelf in the Ross Sea. In order to validate this hypothesis more data (including stable isotopes) of mumiyo and fresh stomach oil from various locations around the continent are needed.

Our study demonstrates that mumiyo deposits are unique records for environmental conditions during the last glacial and provide new insights into the response of the Antarctic fauna under glacial climate conditions. For future studies, systematic sampling and evaluation of mumiyo could provide an extended database that allows for wider inferences about the coastal ecosystem and oceanographic conditions in Antarctica during the past.

#### Acknowledgments

This work was funded by the Deutsche Forschungsgemeinschaft (DFG) in the framework of the priority program “Antarctic Research with comparative investigations in Arctic ice areas” (grant BE 4764/4-1). Data are available on PANGAEA (<https://doi.org/10.1594/PANGAEA.895334>). U. Wand and the field team of the GEOMAUD 97/98 expedition are thanked for sample collection. We thank J. Rethemeyer for <sup>14</sup>C analyses at the Cologne AMS and S. Opitz for TOC analysis in preparation of the project (both University of Cologne). The study was further supported by E. Fernandez Galego (diatom analysis, University of Cologne), P. Grunert and H. Chieszynski (Scanning Electron Microscopy, University of Cologne), and H. Grobe and A. Jaeschke (subsampling of mumiyo deposits, Alfred-Wegener Institute, Bremerhaven). We also thank D. Ainley and B. Davies for their constructive comments on an earlier version of the manuscript.

#### References

- Aiello, A., Fattorusso, E., Menna, M., Vitalone, R., Schröder, H., & Müller, W. (2011). Mumiyo traditional medicine: Fossil deposits from Antarctica (chemical composition and beneficial bioactivity). *Evidence-based Complementary and Alternative Medicine*, 2011, 1–8. <https://doi.org/10.1093/ecam/nen072>
- Ainley, D. G., Hobson, K. A., Crosta, X., Rau, G. H., Wassenaar, L. I., & Augustinus, P. C. (2006). Holocene variation in the Antarctic coastal food web: Linking  $\delta$ D and  $\delta^{13}$ C in snow petrel diet and marine sediments. *Marine Ecology Progress Series*, 306, 31–40. <https://doi.org/10.3354/meps306031>
- Ainley, D. G., O'Connor, E. F., & Boekelheide, R. J. (1984). The marine ecology of birds in the Ross Sea, Antarctica. *Ornithological Monographs*, 32, 97.
- Ainley, D. G., Ribic, C. A., & Fraser, W. R. (1992). Does prey preference affect habitat choice in Antarctic seabirds? *Marine Ecology Progress Series*, 90, 207–221. <https://doi.org/10.3354/meps090207>
- Arrigo, A. K., & van Dijken, G. L. (2003). Phytoplankton dynamics within 37 Antarctic coastal polynya systems. *Journal of Geophysical Research*, 108(C8), 3271. <https://doi.org/10.1029/2002JC001739>
- Ballard, G., Jongsomjit, D., Veloz, S. D., & Ainley, D. G. (2012). Coexistence of mesopredators in an intact polar ocean ecosystem: The basis for defining a Ross Sea marine protected area. *Biological Conservation*, 156, 72–82. <https://doi.org/10.1016/j.biocon.2011.11.017>
- Barbraud, C., & Weimerskirch, H. (2001). Contrasting effects of the extent of sea-ice on the breeding performance of an Antarctic top predator, the snow petrel *Pagodroma nivea*. *Journal of Avian Biology*, 32(4), 297–302. <https://doi.org/10.1111/j.0908-8857.2001.320402.x>
- Barbraud, C., Weimerskirch, H., Guinet, C., & Jouventin, P. (2000). Effect of sea-ice extent on adult survival of an Antarctic top predator: The snow petrel *Pagodroma nivea*. *Oecologia*, 125(4), 483–488. <https://doi.org/10.1007/s004420000481>
- Clark, P. U., Dyke, A. S., Shakun, J. D., Carlson, A. E., Clark, J., Wohlfarth, B., Mitrovica, J. X., et al. (2009). The Last Glacial Maximum. *Science*, 325(5941), 710–714. <https://doi.org/10.1126/science.1172873>
- Clarke, A., & Prince, P. A. (1976). The origin of stomach oil in marine birds: Analyses of the stomach oil from six species of subantarctic procellariiform birds. *Journal of Experimental Marine Biology and Ecology*, 23(1), 15–30. [https://doi.org/10.1016/0022-0981\(76\)90082-4](https://doi.org/10.1016/0022-0981(76)90082-4)
- Connan, M., Cherel, Y., & Mayzaud, P. (2007). Lipids from stomach oil of procellariiform seabirds document the importance of myctophid fish in the Southern Ocean. *Limnology and Oceanography*, 52(6), 2445–2455. <https://doi.org/10.4319/lo.2007.52.6.2445>
- Connan, M., Mayzaud, P., Boutoute, M., Weimerskirch, H., & Cherel, Y. (2005). Lipid composition of stomach oil in a procellariiform seabird *Puffinus tenuirostris*: Implications for food web studies. *Marine Ecology Progress Series*, 290, 277–290. <https://doi.org/10.3354/meps290277>
- Connan, M., Mayzaud, P., Trouve, C., Barbraud, C., & Cherel, Y. (2008). Interannual dietary changes and demographic consequences in breeding blue petrels from Kerguelen Islands. *Marine Ecology Progress Series*, 373, 123–135. <https://doi.org/10.3354/meps07723>
- Croxall, J. P., Steele, W. K., McInnes, S. J., & Prince, P. A. (1995). Breeding distribution of the snow petrel *Pagodroma nivea*. *Marine Ornithology*, 23, 69–99.
- Delord, K., Pinet, P., Pinaud, D., Barbraud, C., De Grissac, S., Lewden, A., Cherel, Y., et al. (2016). Species-specific foraging strategies and segregation mechanisms of sympatric Antarctic fulmarine petrels throughout the annual cycle. *Ibis*, 158(3), 569–586. <https://doi.org/10.1111/ibi.12365>

- Dewald, A., Heinze, S., Jolie, J., Zilges, A., Dunai, T., Rethemeyer, J., Melles, M., et al. (2013). CologneAMS, a dedicated center for accelerator mass spectrometry in Germany. *Nuclear Instruments and Methods in Physics Research B*, 294, 18–23. <https://doi.org/10.1016/j.nimb.2012.04.030>
- Einoder, L. D., Emmerson, L., Southwell, D. M., & Southwell, C. J. (2014). Cavity characteristics and ice accumulation affect nest selection and breeding in snow petrels *Pagodroma nivea*. *Marine Ornithology*, 42, 175–182.
- Emslie, S. D., & Woehler, E. J. (2005). A 9000-year record of Adélie penguin occupation and diet in the Windmill Islands, East Antarctica. *Antarctic Science*, 17(1), 57–66. <https://doi.org/10.1017/S0954102005002427>
- Ferretti, V., Soave, G. E., Casaux, R., & Coria, N. R. (2001). Diet of the snow petrel *Pagodroma nivea* at Laurie Island, Antarctica, during the 1997/98 breeding season. *Marine Ornithology*, 29, 71–73.
- Gao, Y., Wang, J., Xie, Z., Wang, Y., & Sun, L. (2018). Penguin colonization following the last glacial-interglacial transition in the Vestfold Hills, East Antarctica. *Palaeogeography, Palaeoclimatology, Palaeoecology*, 490, 629–639. <https://doi.org/10.1016/j.palaeo.2017.11.053>
- Gersonde, R., Crosta, X., Abelman, A., & Armand, L. (2005). Sea-surface temperature and sea ice distribution of the Southern Ocean at the EPILOG Last Glacial Maximum—A circum-Antarctic view based on siliceous microfossil records. *Quaternary Science Reviews*, 24(7–9), 869–896. <https://doi.org/10.1016/j.quascirev.2004.07.015>
- Goldworthy, P. M., & Thomson, P. G. (2000). An extreme inland breeding locality of snow petrels (*Pagodroma nivea*) in the southern Prince Charles Mountains, Antarctica. *Polar Biology*, 23(10), 717–720. <https://doi.org/10.1007/s003000000146>
- Hammer, Ø., Harper, D. A. T., & Ryan, P. D. (2001). PAST: Paleontological statistics software package for education and data analysis. *Palaeontologica Electronica*, 4, 9p
- Hansen, R. P., & Meiklen, S. M. (1970). Isoprenoid fatty acids in Antarctic krill (*Euphausia superba*). *Journal of the Science of Food and Agriculture*, 21(4), 203–206. <https://doi.org/10.1002/jsfa.2740210409>
- Haus, N. W., Wilhelm, K. R., Bockheim, J. G., Fournelle, J., & Miller, M. (2016). A case for chemical weathering in soils of Hurd Peninsula, Livingston Island, South Shetland Islands, Antarctica. *Geoderma*, 263, 185–194. <https://doi.org/10.1016/j.geoderma.2015.09.019>
- Hiller, A., Hermichen, W. D., & Wand, U. (1995). Radiocarbon-dated subfossil stomach oil deposits from petrel nesting sites; novel paleoenvironmental records from continental Antarctica. *Radiocarbon*, 37(02), 171–180. <https://doi.org/10.1017/S0033822200030617>
- Hiller, A., Wand, U., Kämpf, H., & Stackedbrandt, W. (1988). Occupation of the Antarctic continent by petrels during the past 35000 years: Inferences from a  $^{14}\text{C}$  study of stomach oil deposits. *Polar Biology*, 9(2), 69–77. <https://doi.org/10.1007/BF00442032>
- Höfle, S., Rethemeyer, J., Mueller, C. W., & John, S. (2013). Organic matter composition and stabilization in a polygonal tundra soil of the Lena Delta. *Biogeosciences*, 10(5), 3145–3158. <https://doi.org/10.5194/bg-10-3145-2013>
- Huang, T., Sun, L., Wang, Y., Liu, X., & Zhu, R. (2008). Penguin population dynamics for the past 8500 years at Gardner Island, Vestfold Hills. *Antarctic Science*, 21(6), 571. <https://doi.org/10.1017/S0954102009990332>
- Kiernan, K., Gore, D. B., Fink, D., White, D. A., McConnell, A., & Sigurdsson, I. A. (2009). Deglaciation and weathering of Larsemann Hills, east Antarctica. *Antarctic Science*, 21(4), 373–382. <https://doi.org/10.1017/S0954102009002028>
- Kiernan, K., McConnell, A., & Lawson, E. (2002). Radiocarbon dating of mumiyo from the Vestfold Hills, East Antarctica. *Papers and Proceedings of the Royal Society of Tasmania*, 136, 141–144.
- Lea, M.-A., Nichols, P. D., & Wilson, G. (2002). Fatty acid composition of lipid-rich myctophids and mackerel icefish (*Champsocephalus gunnari*)—Southern Ocean food-web implications. *Polar Biology*, 25, 843–854.
- Lindeboom, H. J. (1984). The nitrogen pathway in a penguin rookery. *Ecology*, 65(1), 269–277. <https://doi.org/10.2307/1939479>
- Liu, X., Nie, Y., Sun, L., & Emslie, S. D. (2013). Eco-environmental implications of elemental and carbon isotope distributions in ornithogenic sediments from the Ross Sea region, Antarctica. *Geochimica et Cosmochimica Acta*, 117, 99–114. <https://doi.org/10.1016/j.gca.2013.04.013>
- Mackintosh, A., Golledge, N., Domack, E., Dunbar, R., Leventer, A., White, D., Pollard, D., et al. (2011). Retreat of the East Antarctica ice sheet during the last glacial termination. *Nature Geoscience*, 4(3), 195–202. <https://doi.org/10.1038/ngeo1061>
- Melles, M., Kulbe, T., Verkulich, S. R., Pushina, Z. V., & Hubberten, H.-W. (1997). Late Pleistocene and Holocene environmental history of Bunge Hills, East Antarctica, as revealed by fresh-water and epishelf lake sediments. In C. A. Ricci (Ed.), *The Antarctic region: Geological evolution and processes* (pp. 809–820). Siena: Terra Antarctica Publication.
- Mychra, A., & Tatur, A. (1991). Ecological role of the current and abandoned penguin rookeries in the land environment of the maritime Antarctic. *Polish Polar Research*, 12, 3–24.
- Nichols, D. S., Nichols, P. D., & Sullivan, W. (1993). Fatty acid, sterol and hydrocarbon composition of Antarctic sea ice diatom communities during the spring bloom in McMurdo Sound. *Antarctic Science*, 5, 271–278.
- Pereira, T. T. C., Schaefer, C. E. G. R., Ker, J. C., Almeida, C. C., Almeida, I. C. C., & Pereira, A. B. (2013). Genesis, mineralogy and ecological significance of ornithogenic soils from a semi-desert polar landscape at Hope Bay, Antarctic Peninsula. *Geoderma*, 209–210, 98–109. <https://doi.org/10.1016/j.geoderma.2013.06.012>
- Phillips, K. L., Nichols, P. D., & Jackson, G. D. (2002). Lipid and fatty acid composition of the mantle and digestive gland of four Southern Ocean squid species: Implications for food-web studies. *Antarctic Science*, 14, 212–220.
- Phleger, C. F., Nelson, M. M., Mooney, B. D., & Nichols, P. D. (2002). Inter-annual and between species comparison of the lipids, fatty acids and sterols of Antarctic krill from the US AMLR Elephant Islands survey area. *Comparative Biochemistry and Physiology: Part B*, 131(4), 733–747. [https://doi.org/10.1016/S1096-4959\(02\)00021-0](https://doi.org/10.1016/S1096-4959(02)00021-0)
- Phleger, C. F., Nichols, P. D., & Virtue, P. (1997). The lipid, fatty acid and fatty alcohol composition of the myctophid fish *Electrona antarctica*: High level of wax esters and food-chain implications. *Antarctic Science*, 9, 258–265.
- Polach, H. A., Gower, J., & Fraser, I. (1972). Synthesis of high purity benzene for radiocarbon dating by liquid scintillation method. In T. A. Rafter & T. Taylor (Eds.), *Proceedings of the 8th international  $^{14}\text{C}$  conference* (pp. 145–157). Wellington: Royal Society of New Zealand.
- Quillfeldt, P., Masello, J. F., Brickley, P., & Martin-Creuzburg, D. (2011). Fatty acid signatures of stomach content reflect inter- and intra-annual changes in diet of a small pelagic seabird, the thin-billed prion *Pachyptila belcheri*. *Marine Biology*, 158(8), 1805–1813. <https://doi.org/10.1007/s00227-011-1693-8>
- Reimer, P. J., Bard, E., Bayliss, A., Beck, J. W., Blackwell, P. G., Bronk Ramsey, C., et al. (2013). INTCAL13 and Marine13 radiocarbon age calibration curves 0–50,000 years cal BP. *Radiocarbon*, 55(4), 1869–1887. [https://doi.org/10.2458/azu\\_js\\_rc.55.16947](https://doi.org/10.2458/azu_js_rc.55.16947)
- Roberts, S. J., Monien, P., Foster, L. C., Loftfield, J., Hocking, E. P., Schnetger, B., Pearson, E. J., et al. (2017). Past penguin colony responses to explosive volcanism on the Antarctic Peninsula. *Nature Communications*, 8. <https://doi.org/10.1038/ncomms14914>
- Ryan, P. G., Steele, W. K., Siegfried, W. R., & Vogel, J. C. (1992). Radiocarbon-dates of snow petrel regurgitations can reveal exposure periods for nunataks in Antarctica. *South African Journal of Science*, 88, 578–590.
- Smith, J. A., Hillenbrand, C.-D., Pudsey, C. J., Allen, C. S., & Graham, A. G. C. (2010). The presence of polynyas in the Weddell Sea during the Last Glacial Period with implications for the reconstruction of sea-ice limits and ice sheet history. *Earth and Planetary Science Letters*, 296(3–4), 287–298. <https://doi.org/10.1016/j.epsl.2010.05.008>

- Sprenk, D., Weber, M. E., Kuhn, G., Wennrich, V., Hartmann, T., & Seelos, K. (2014). Seasonal changes in glacial polynya activity inferred from Weddell Sea varves. *Climate of the Past*, 10(3), 1239–1251. <https://doi.org/10.5194/cp-10-1239-2014>
- Steele, W. K., & Hiller, A. (1997). Radiocarbon dates of snow petrel (*Pagodroma nivea*) nest sites in central Dronning Maud Land, Antarctica. *Polar Record*, 33(184), 29–38. <https://doi.org/10.1017/S0032247400014145>
- Steele, W. K., & Newton, I. P. (1995). New distribution and breeding records of birds in the Ahlmannryggen, western Dronning Maud Land, Antarctica, 1991–1995. *Marine Ornithology*, 23, 47–52.
- Stuiver, M., & Reimer, P. J. (1993). Extended  $^{14}\text{C}$  database and revised CALIB 3.0  $^{14}\text{C}$  age calibration program. *Radiocarbon*, 35(01), 215–230. <https://doi.org/10.1017/S0033822200013904>
- Thatje, S., Hillenbrand, C.-D., Mackensen, A., & Larter, R. (2008). Life hung by a thread: Endurance of Antarctic fauna in glacial periods. *Ecology*, 89(3), 682–692. <https://doi.org/10.1890/07-0498.1>
- Thor, G., & Low, M. (2011). The persistence of the snow petrel (*Pagodroma nivea*) in Dronning Maud land (Antarctica) for over 37,000 years. *Polar Biology*, 34(4), 609–613. <https://doi.org/10.1007/s00300-010-0912-y>
- Verkulich, S. R., & Hiller, A. (1994). Holocene deglaciation of the Bunger Hills revealed by  $^{14}\text{C}$  measurements on stomach oil deposits in snow petrel colonies. *Antarctic Science*, 6, 395–399.
- Wacker, L., Nemec, M., & Bourquin, J. (2010). A revolutionary graphitisation system: Fully automated, compact and simple. *Nuclear Instruments and Methods in Physics Research B*, 268(7-8), 931–934. <https://doi.org/10.1016/j.nimb.2009.10.067>
- Wand, U., & Hermichen, W. D. (2005). Late Quaternary ice level changes in central Dronning Maud Land, East Antarctica, as inferred by  $^{14}\text{C}$  ages of mumiyo deposits in snow petrel colonies. *Geologisches Jahrbuch*, 97, 237–254.
- Warham, J. (1977). The incidence, functions and ecological significance of petrel stomach oils. *Proceedings of the New Zealand Ecological Society*, 24, 84–93.
- Warham, J., Watts, R., & Dainty, R. J. (1976). The composition, energy content and function of the stomach oils of petrels (order procel-lariiformes). *Journal of Experimental Marine Biology and Ecology*, 23(1), 1–13. [https://doi.org/10.1016/0022-0981\(76\)90081-2](https://doi.org/10.1016/0022-0981(76)90081-2)
- Watts, R., & Warham, J. (1976). Structure of some intact lipids of petrel stomach oils. *Lipids*, 11(6), 423–429. <https://doi.org/10.1007/BF02532831>
- Williams, C. T., & Buck, C. L. (2010). Using fatty acids as dietary tracers in seabird trophic ecology: Theory, applications and limitations. *Journal of Ornithology*, 151(3), 531–543. <https://doi.org/10.1007/s10336-010-0513-0>
- Younger, J. L., Emmerson, L. M., & Miller, K. J. (2016). The influence of historical climate changes on Southern Ocean marine predator populations: A comparative analysis. *Global Change Biology*, 22(2), 474–493. <https://doi.org/10.1111/gcb.13104>
- Zielinski, U., & Gersonde, R. (1997). Diatom distribution in the Southern Ocean surface sediments (Atlantic sector): Implications for paleoenvironmental reconstructions. *Palaeogeography, Palaeoclimatology, Palaeoecology*, 129(3-4), 213–250. [https://doi.org/10.1016/S0031-0182\(96\)00130-7](https://doi.org/10.1016/S0031-0182(96)00130-7)